Annals of Botany **125**: 833–840, 2020
doi: 10.1093/aob/mcz192, available online at www.academic.oup.com/aob

ANNALS OF BOTANY
Founded 1887

PART OF THE FOCUS ISSUE ON PLANT DEFENCE AND STRESS REPSONSE

Three-dimensional ultrastructural change of chloroplasts in rice mesophyll cells responding to salt stress

Takao Oi[1,*], Sakiko Enomoto[2], Tomoyo Nakao[2], Shigeo Arai[2], Koji Yamane[3] and Mitsutaka Taniguchi[1]

[1]Graduate School of Bioagricultural Sciences, Nagoya University, Nagoya 464-8601, Japan, [2]High Voltage Electron Microscope Laboratory, Institute of Materials and Systems for Sustainability, Nagoya University, Nagoya 464-8601, Japan and [3]Graduate School of Agriculture, Kindai University, Nara 631-8505, Japan
**For correspondence. E-mail: oitaka@agr.nagoya-u.ac.jp*

Received: 28 August 2019 Returned for revision: 8 October 2019 Editorial decision: 19 November 2019 Accepted: 26 November 2019
Published electronically 27 November 2019

• **Background and Aims** Excess salinity inhibits the metabolism of various systems and induces structural changes, especially in chloroplasts. Although the chloroplast body seems to swell under salinity stress as observed by conventional transmission electron microscopy, previous studies are limited to 2-D data and lack quantitative comparisons because specimens need to be sliced into ultrathin sections. This study shows three-dimensionally the structural changes in a whole mesophyll cell responding to salinity stress by serial sectioning with a focused ion beam scanning electron microscope (FIB-SEM) and compares the differences in chloroplast structures based on reconstructed models possessing accurate numerical voxel values.
• **Methods** Leaf blades of rice plants treated with 100 mM NaCl or without (control) for 4 d were fixed chemically and embedded in resin. The specimen blocks were sectioned and observed using the FIB-SEM, and then the sliced image stacks were reconstructed into 3-D models by image processing software.
• **Key Results** On the transverse sections of rice mesophyll cells, the chloroplasts in the control leaves appeared to be elongated meniscus lens shaped, while those in the salt-treated leaves appear to be expanded oval shaped. The 3-D models based on serial sectioning images showed that the chloroplasts in the control cells spread like sheets fitted to the shape of the cell wall and in close contact with the adjacent chloroplasts. In contrast, those in the salt-stressed cells curled up into a ball and fitted to cell protuberances without being in close contact with adjacent chloroplasts. Although the shapes of chloroplasts were clearly different between the two treatments, their volumes did not differ.
• **Conclusions** The 3-D reconstructed models of whole rice mesophyll cells indicated that chloroplasts under salt stress conditions were not swollen but became spherical without increasing their volume. This is in contrast to findings of previous studies based on 2-D images.

Keywords: Chloroplast, chloroplast protrusion, focused ion beam scanning electron microscope, mesophyll cell, *Oryza sativa* L., salt stress, three-dimensional reconstruction, ultrastructure, transmission electron microscope.

INTRODUCTION

Salt accumulation in soil (soil salinization) is one of the most serious environmental factors limiting the growth and yield of crops (Hillel, 2000). Excess salinity inhibits various metabolisms, including photosynthesis (Parida and Das, 2005), and induces ultrastructural changes, especially in chloroplasts, which appear to be the most affected by salt stress (Rahman *et al*., 2000; Mitsuya *et al*., 2003*a*; Yamane *et al*., 2003, 2008, 2012).

Under severe salinity stress, swelling and degradation of thylakoids have been observed (Rahman *et al*., 2000; Mitsuya *et al*., 2003*a*; Yamane *et al*., 2003, 2004). These changes are induced by the accumulation of reactive oxygen species (ROS) derived from excess reductants (Yamane *et al*., 2004) when carbon fixation ability is reduced owing to stomatal closure in response to osmotic stress caused by high salinity in soil (Chaves *et al*., 2009). The destruction of the chloroplast envelope has also been observed and is considered to be caused by osmotic stress (Yamane *et al*., 2003). In addition, tubular projections of chloroplasts, termed stromules (Köhler and Hanson, 2000; Gray *et al*., 2012) or chloroplast protrusions (Bourett *et al*., 1999; Yamane *et al*., 2012), are formed under salt stress. It has been suggested that the formation of the chloroplast protrusion is followed by the ejection of a Rubisco-containing body (Chiba *et al*., 2003), which is isolated from the chloroplast body, and that this may be one of the pathways for chloroplast degradation under salt stress (Yamane *et al*., 2012; Ishida *et al*, 2014). In addition, the chloroplast body also seems to swell with salinity, not only under high salt concentrations or long-term treatment (Rahman *et al*., 2000) but also under mild concentrations (see fig. 3b in Yamane *et al*., 2008) or in the early stage of treatment (see fig. 3A in Yamane *et al*., 2003); however, the chloroplast volume has not been compared quantitatively.

As mentioned above, numerous studies on chloroplast structures under salinity stress have been reported; however, there are few studies showing their 3-D structural changes. Because the conventional transmission electron microscope (TEM) observations, which have been used in previous studies, require

© The Author(s) 2019. Published by Oxford University Press on behalf of the Annals of Botany Company.
All rights reserved. For permissions, please e-mail: journals.permissions@oup.com.

the specimens to be sliced into ultrathin sections (approx. 0.1 µm), it is difficult to comprehend the 3-D structure intuitively. There are also few studies that investigated changes in organelle volume in response to salinity stress. In addition, the TEM observation tends to focus attention on the region near the centre of the cell to take representative images of the cell. The peripheral regions of the cell have often been overlooked; however, it is important to observe a whole cell from the centre to the peripheral regions in order to understand the cell structure comprehensively.

Originally, sectional images are restricted to 2-D data; however, stacking the micrographs of serial sections provides 3-D volume data. Recently, several types of electron microscopy have been proposed for the reconstruction of 3-D structures from micrographs of serial sections (Hughes *et al*., 2014). One of the tools used to reconstruct the 3-D ultrastructure is a focused ion beam (FIB) scanning electron microscope (SEM) (FIB-SEM) (Knott *et al*., 2008). The FIB-SEM provides hundreds of sectioning images at correct intervals at the nanometre scale, and then image processing software can convert the image stacks into virtual cross-sections at every conceivable angle or depth and into the 3-D reconstructed models of cell components (Lucas *et al*., 2012).

Recently, we visualized the ultrastructure of a whole rice mesophyll cell by 3-D reconstruction based on serial sectioning 2-D images obtained with the FIB-SEM (Oi *et al*., 2017). The reconstructed models include 3-D information at the ultrastructural level with accurate values for volume and surface area. In our previous study, this method showed that unstressed rice mesophyll cells are discoid shaped with several lobes around the cell periphery, increasing the surface area to volume ratio, and the chloroplasts occupied half of the cell volume and spread as sheets along the cell lobes, covering most of the inner cell surface (Oi *et al*., 2017). It is considered that rice mesophyll cells with increased cell surface area and sheet-shaped chloroplasts enhance CO_2 absorption (Sage and Sage, 2009; Oi *et al*., 2017).

In this study, we used the FIB-SEM followed by 3-D reconstruction to investigate ultrastructural changes in rice mesophyll cells, especially chloroplasts, associated with salinity stress. Here we discuss the 3-D morphological changes in chloroplasts based on reconstructed models with accurate numerical voxel values.

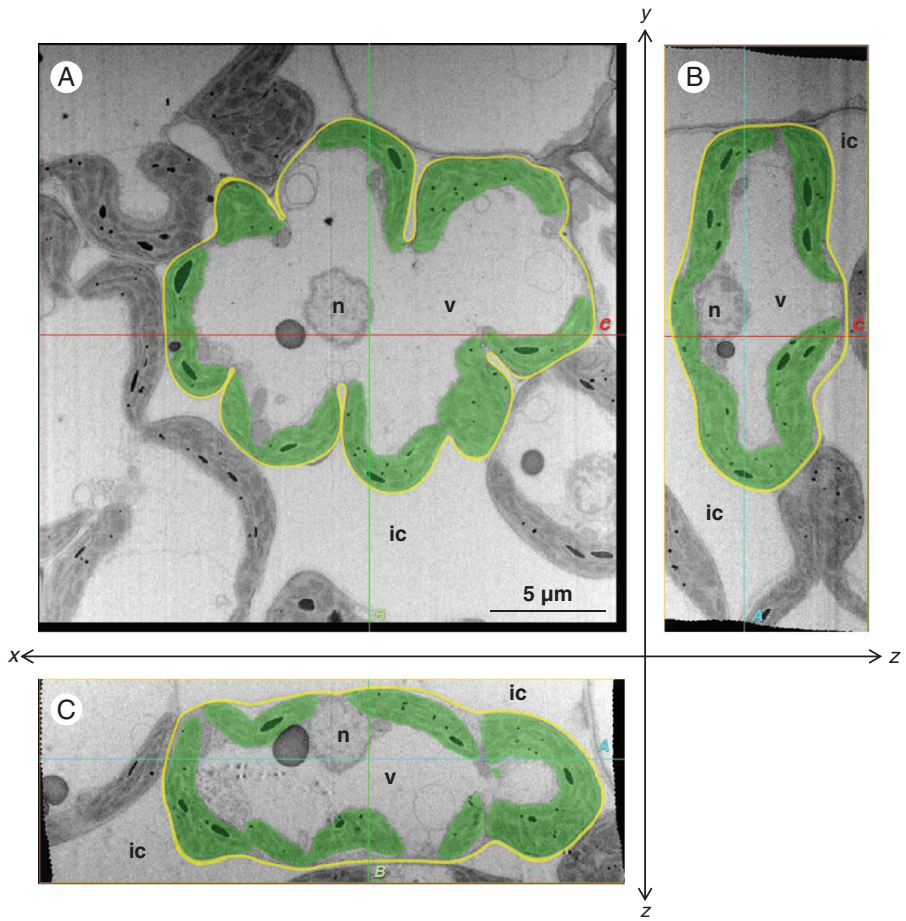

FIG. 1. Central cross-sections of the mesophyll cells of the rice leaf blade in the control plant. (A) *xy*-transversal sections obtained with the focused ion beam scanning electron microscope. One image in a sequence of sections for a whole mesophyll cell: 107th in the sequence of 177. (B, C) Orthogonal slice images virtually imaged with the plugin 'Volume Viewer' of the software 'Fiji'. (B) *yz*-orthogonal sections of the image stacks. (C) *xz*-orthogonal sections of the image stacks. Each slice plane (A, B, C) crosses the lines marked '*A*, *B* and *C*' shown in the other orientational images. All images were segmented manually: green, chloroplast; yellow, cell wall; ic, intercellular space; n, nucleus; v, vacuole. Cutting interval (*z*-step) = 50 nm.

MATERIALS AND METHODS

Plant material and growth conditions

Caryopses of rice (*Oryza sativa* L. 'Nipponbare') were imbibed in a beaker containing distilled water in an incubation room at 30 ± 2 °C. After the white tip of the coleoptile appeared, the caryopses were sown on a mesh above a plastic bucket containing nutrient solution (Mae and Ohira, 1981). The seedlings were cultivated hydroponically in a growth chamber under a daily 14 h photoperiod at 500 µmol m^{-2} s^{-1} with 28/20 °C (day/night), for 21 d. Then, they were treated with 100 mM NaCl in the nutrient solution for 4 d. Control plants were grown in the nutrient solution without NaCl.

Specimen preparation

The uppermost fully expanded (fifth–seventh) leaves were chemically fixed and embedded in resin as described in Oi *et al.* (2017). Small segments (approx. 1 × 2 mm) excised from the middle portion of the leaf blades were vacuum-infiltrated for 5 min in Karnovsky's fixative (mixture of 4 % paraformaldehyde and 5 % glutaraldehyde) in 50 mM sodium phosphate buffer (pH 7.2) and pre-fixed in the same solution for 5 h. After being rinsed in the buffer for 2 h, the segments were post-fixed in 2 % osmium tetroxide in the same buffer for 12 h. The segments were rinsed with the buffer and distilled water, dehydrated in a graded acetone series (30, 50, 70, 90, 99 and 100 %), treated with propylene oxide and then embedded in Spurr's resin.

FIB-SEM observation

The leaf segments embedded in resin were serially cut and observed with a FIB-SEM according to Oi *et al.* (2017). Transverse section of the embedded leaf segments were exposed using a diamond knife on an ultramicrotome (EM UC6, Leica, Germany). The resin blocks were subsequently trimmed to a cuboid (approx. 3 × 3 × 2 mm) and glued to the standard specimen stage for FIB-SEM. The transverse section of the leaf

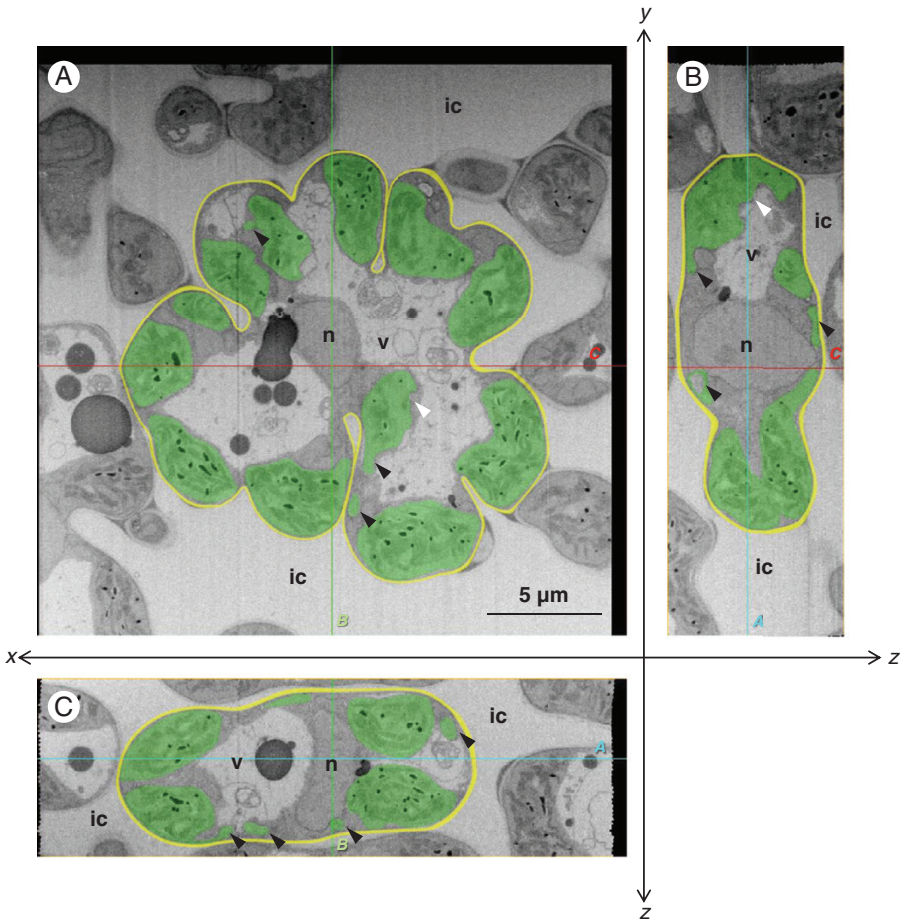

FIG. 2. Central cross-sections of the mesophyll cells of the rice leaf blade in the NaCl-treated plants. (A) *xy*-transversal sections obtained with the focused ion beam scanning electron microscope. One image in a sequence of sections for a whole mesophyll cell: 84th in the sequence of 154. (B, C) Orthogonal slice images virtually imaged with the plugin 'Volume Viewer' of the software 'Fiji'. (B) *yz*-orthogonal sections of the image stacks. (C) *xz*-orthogonal sections of the image stacks. Each slice plane (A, B and C) crosses the lines marked '*A*, *B* and *C*' shown in the other orientational images. All images were segmented manually: green, chloroplast; yellow, cell wall; ic, intercellular space; n, nucleus; v, vacuole. White arrowheads indicate the partly distorted portion of the chloroplast envelope. Black arrowheads indicate the chloroplast protrusions or vesicles. Cutting interval (*z*-step) = 50 nm.

faced the SEM column, and the leaf veins in the segment were placed vertically to the FIB column. The specimens were coated with a thin layer of evaporated carbon with a carbon coater (CADE-EMT, Meiwafosis, Japan) to prevent electron charging. Serial electron micrographs were obtained with a FIB-SEM (MI-4000L, Hitachi, Japan), in which the FIB and SEM columns were orthogonally arranged; the angle of the two columns was 90°. Specimen surfaces were exposed using the FIB, and then block-face images were captured with the SEM. Serial electron micrographs were obtained automatically by repetitive cutting with the FIB and image capturing with the SEM. The FIB was operated as follows: an accelerating voltage, 30 kV; a beam current for milling to prepare or to cut, repetitively, 1.6 or 1.2 nA, respectively; cutting interval, 50 nm. The SEM was operated as follows: accelerating voltage, 1.0 kV; working distance, 2 mm; dwell time, 30 µs per pixel; image size, 1000 × 1000 pixels; colour depth, 8-bit (256 grey scales); pixel size, 25 (or 20, only for NaCl-treated plant #3) nm per pixel; beam current, 10 pA (±10 %). Secondary electrons were detected by the upper detector in the SEM column. Backscattered electrons were also detected, but we did not use them for imaging in this study.

3-D reconstruction

The resultant image stacks from the block-face imaging were processed using the software 'Fiji' (http://fiji.sc/Fiji) (Schindelin *et al*., 2012); grey scale was inverted so that the SEM images resembled TEM images, brightness and contrast were adjusted and then the slices were aligned. The processed 2-D image stacks were then compiled into orthogonal slice images by volume rendering with the plugin 'Volume Viewer' of Fiji. The regions of cell walls and chloroplasts in all 2-D images (actual cross-sections) were also segmented using the software 'PaintTool SAI' (ver. 1, Systemax, Japan); each component was manually painted with a specified colour and saved in BMP format (colour depth: 24 bit). The colour-segmented image stacks were then reconstructed into 3-D models by surface rendering, using the software 'Image-Pro Premier 3D' (ver. 9.3, Media Cybernetics, USA). The 3-D rendered models were smoothed with the 'Low-pass filter' (3 × 3 × 3), and then their volume, surface area and sphericity were calculated with the function '3D Measure' of Image-Pro Premier 3D.

Statistical analysis

The data were statistically analysed using Microsoft Excel with add-in software (Statcel 3, OMS Publishing Inc., Japan). Means were compared by Student's *t*-test, and medians were compared by Mann–Whitney's *U*-test (*$P < 0.05$, **$P < 0.01$). Other details regarding statistical parameters can be found in the figure legends.

RESULTS

The transverse sections at the centre of the rice mesophyll cells showed that the cells were lobed with several invaginations in both the control and NaCl-treated leaves (Figs 1A and 2A). In control leaves, the meniscus-lens-shaped chloroplasts were distributed along the lobed cell wall (Fig. 1A). Conversely, in NaCl-treated leaves, the chloroplasts expanded into an oval shape (Fig. 2A). The paradermal and longitudinal sections also showed meniscus-lens-shaped chloroplasts in the control leaves and expanded oval chloroplasts in the NaCl-treated leaves, even though the sections showed an oblong cell shape without deep invaginations (Figs 1B, C and 2B, C). Although the chloroplast envelope was partly distorted in the NaCl-treated cells (Fig. 2; white arrowheads), the swelling or degradation of thylakoids was not observed in either the control or NaCl-treated leaves (Figs 1 and 2). The sections in the NaCl-treated cells showed several protrusions and vesicles of chloroplast (Fig. 2: black arrowheads); however, they continuously connected with chloroplast bodies in serial image stacks. All slice data are shown in Supplementary data Videos 1–6.

The cell walls of mesophyll cells in the serial images were segmented and reconstructed into 3-D models (Fig. 3). Although there was some variation in the shape of these cells, they were generally bumpy discoid with lateral protuberances in both the control and NaCl-treated plants. Cell volume and surface area were calculated based on these 3-D models, and there were no significant differences between the control and NaCl-treated plants in terms of volume ($P = 0.17$) or surface area ($P = 0.33$) of the cells (Table 1).

The chloroplasts in the mesophyll cells were also reconstructed into 3-D models (Fig. 4A). They were distributed along the contour of the cells. The average number of chloroplasts contained in one mesophyll cell was 14.7 ± 2.1 (mean ± s.d.) in the control and 12.3 ± 2.3 (mean ± s.d.) in the NaCl-treated cells; there was no significant difference between the two treatments ($P = 0.26$). Chloroplasts varied in size, and surface area was positively correlated with volume in the control ($R^2 = 0.90$) and NaCl-treated plants ($R^2 = 0.88$) (Fig. 4B). The chloroplast volume did not differ between the control and NaCl-treated plants ($P = 0.11$) (Fig. 5A). However, the surface area (Fig. 5B, $P < 0.05$) and the ratio of surface area to volume

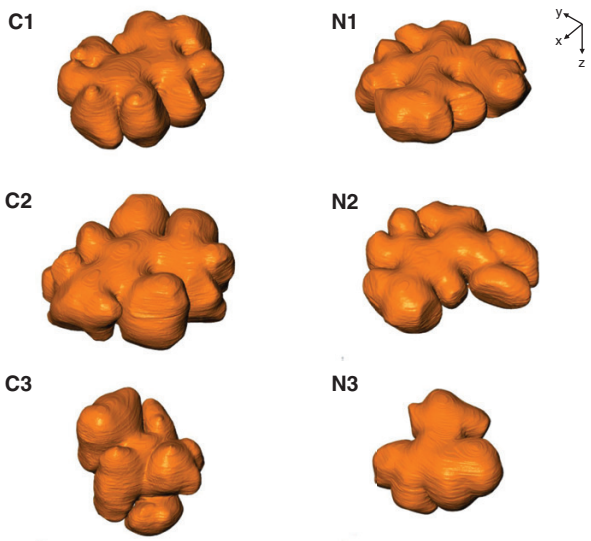

FIG. 3. The 3-D models of rice mesophyll cells in the control (C1–C3) and NaCl-treated (N1–N3) plants. 3-D surface modelling of the cell wall of mesophyll cells shows concave–convex exteriors. Cutting interval = 50 nm; total number of cuttings = 177 (C1), 189 (C2), 297 (C3), 154 (N1), 168 (N2) and 210 (N3).

TABLE 1. *Volume (V), surface area (S) and the ratio of surface area to volume (S/V) of the rice mesophyll cells shown in Fig. 3.*

Control	V (μm³)	S (μm²)	S/V (μm⁻¹)	Salt stress	V (μm³)	S (μm²)	S/V (μm⁻¹)
#1*	1284	799	0.62	#1	1165	812	0.70
#2	1644	995	0.61	#2	1046	746	0.71
#3	1067	694	0.65	#3	795	516	0.65
Mean	1332	830	0.63	Mean	1002	691	0.69
± s.d.	291	153	0.02	± s.d.	189	155	0.03

Means were compared between the control and NaCl-treated plants by Student's *t*-test; V ($P = 0.17$), S ($P = 0.33$), S/V ($P = 0.03$).

*The original serial sectioning images of control plant #1 were the same as the images used in Oi *et al.* (2017). The values of V and S in the previous study were calculated without smoothing the 3-D reconstructed model, and V of the previous model was similar (1280) to the present value; however, S of the previous model was higher (1213) than that of the present study.

(Fig. 5C, $P < 0.01$) were significantly lower in the NaCl-treated plants than in the control plants. There was also a clear difference in the shape of chloroplasts between the two treatments. The chloroplasts in the control cells spread like sheets fitted to the shape of the cell wall with the adjacent chloroplasts in close contact with each other (Fig. 5D). Conversely, those in the NaCl-treated cells curled up into a ball fitted to the cell protuberances without close contact with adjacent chloroplasts (Fig. 5E). To compare the structural changes in chloroplasts between the two treatments, the sphericity of each chloroplast was calculated (Fig. 5F). The sphericity indicates how closely the shape of the object approaches that of a perfect sphere (1.00). The sphericity of the chloroplasts in the NaCl-treated cells (median 0.77) was significantly higher than that in the control cells (median 0.67) (Fig. 5F).

DISCUSSION

The images of cross-sections obtained in this study showed that chloroplasts in salt-stressed mesophyll cells seemed to swell (Fig. 2), the same as found in the previous studies based on TEM observations (e.g. Rahman *et al.*, 2000). However, the 3-D reconstructed models showed that the chloroplasts did not swell but became spherical without increasing in volume (Figs 4 and 5). Therefore, the view that chloroplast swelling (increasing volume) in response to osmotic pressure from salinity stress was based on misinterpretations of 2-D images. The use of 3-D data in the present study overturns the conventional view. Here we discuss the morphology of rice mesophyll cells based on these new 3-D images.

Mesophyll cells in rice leaf blades were a bumpy discoid shape with lateral protuberances (Fig. 3). The mesophyll cells were joined together by their lobes that vary in size and number (Chonan, 1967; Sage and Sage, 2009). The constrictions in the lobes were deep in the transverse (*xy*-) section, and the cell shapes generally seemed to be discoid (Fig. 3). One of the observed cells (Fig. 3C3) was not discoid but rather of an irregular shape; this cell was adjacent to a large epidermal cell on the abaxial leaf side. It seemed that the mesophyll cells in the exterior of the leaf tissue were more irregular in shape than those in the interior. Although cell shape was diverse, it is considered that the external form of the mesophyll cells was unaffected by salinity stress in this experiment (Fig. 3). The cell volume and surface area were not different between the control and salt-stressed cells (Table 1). In this study, we examined the

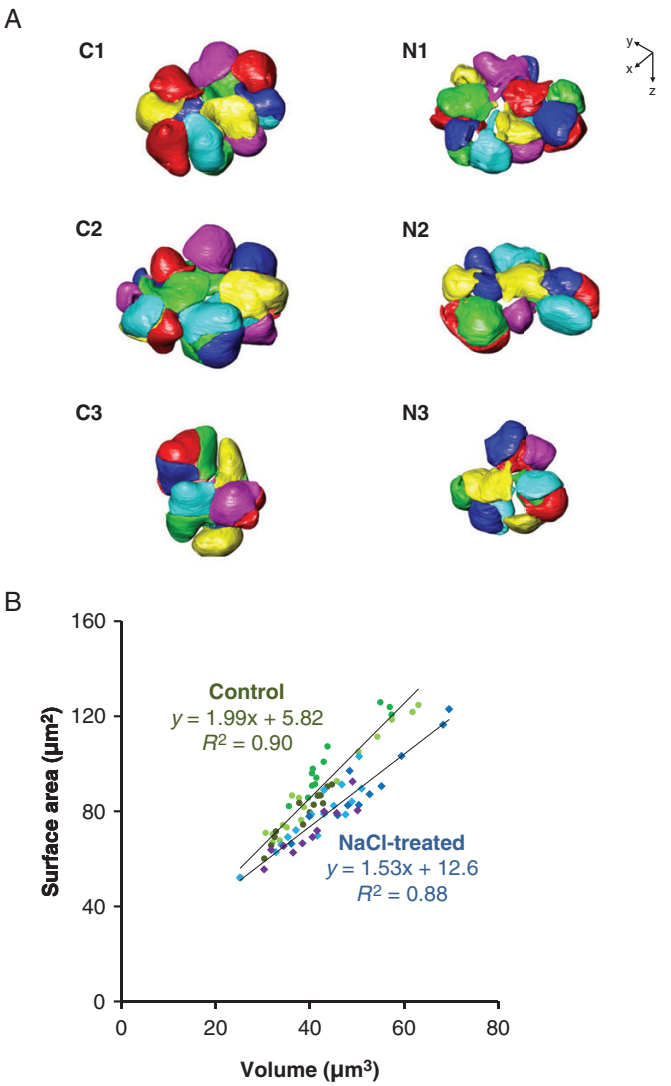

FIG. 4. The 3-D models of the chloroplasts in the rice mesophyll cells in the control (C1–C3) and NaCl-treated (N1–N3) plants. (A) 3-D surface modelling of the chloroplasts shows their configuration in the mesophyll cells, as shown in Fig. 3. Each chloroplast is presented in one colour, and six colours are used to distinguish the neighbouring chloroplasts. The number of chloroplasts contained in each cell was: 13 (C1), 17 (C2), 14 (C3), 15 (N1), 11 (N2) and 11 (N3). (B) Relationship between volume and surface area of the chloroplasts presented. Circles, control ($n = 44$); squares, NaCl treated ($n = 37$). Each symbol with the same colour belongs to the same cell.

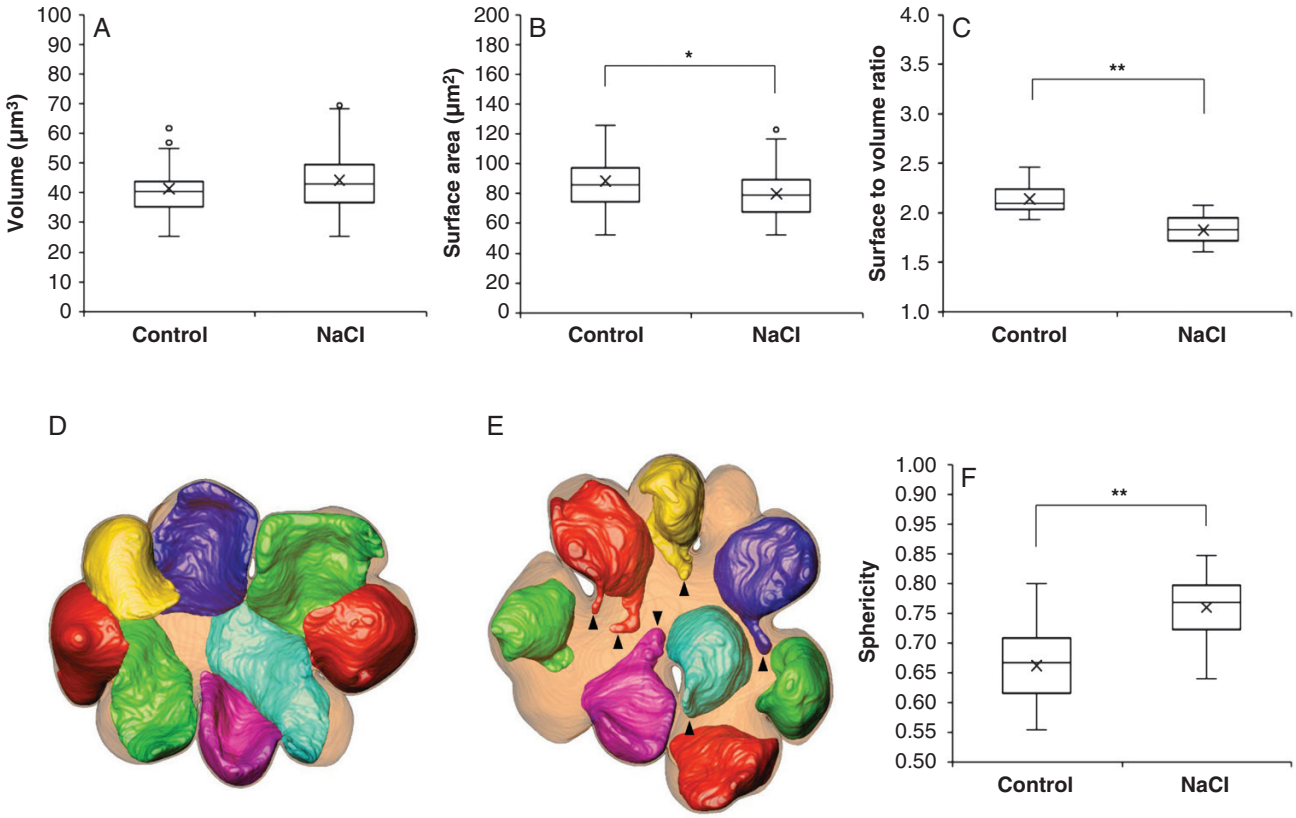

FIG. 5. Size and shape of the chloroplasts in the rice mesophyll cells. (A–C, F) Quantitative analysis of chloroplasts in the three control cells ($n = 44$) and in the three NaCl-treated cells ($n = 37$). Volume (A), surface area (B), the ratio of surface to volume (C) and sphericity (F). Boxes represent the median value and the first and third quartiles; whiskers represent the minimum and maximum values. Medians of the control and NaCl-treated plants were compared by Mann–Whitney's *U*-test (*$P < 0.05$, **$P < 0.01$). (D, E) Top views in parallel with transverse (*xy*) sections showing the 3-D models of chloroplasts in mesophyll cells. (D) control (C1 in Figs 3 and 4), (E) NaCl-treated (N1 in Figs 3 and 4) plants. Translucent blown colour, cell wall; non-transparent colours, chloroplasts. To show their configuration clearly, the seven chloroplasts in the back in the *z*-axial direction are displayed, and the rest of chloroplasts in the front are not displayed. Arrowheads indicate the chloroplast protrusions.

leaves that had fully expanded before the treatments started and had not wilted by the end of the treatment; therefore, it is considered that the cells had not yet greatly dehydrated and shrunk.

Chloroplasts with various shapes were distributed along the complicated cell wall, and it is difficult to understand the difference in chloroplast shape between the two treatments from the perspective of a whole cell (Fig. 4). However, there are clear differences between the control and salt-stressed plants in terms of shape and location of the individual chloroplasts. The chloroplasts in control plants spread like sheets along the lobed cell wall and were in close contact with each other, as previously described (Oi *et al*., 2017) (Fig. 5D). Conversely, we observed that chloroplasts in the salt-stressed cells were significantly more spherical and were not in close contact with adjacent chloroplasts (Fig. 5E). Two possibilities are conceivable regarding the physiological significance of the morphological change under salt stress.

First, the sheet shape of the chloroplasts in the control leaves could be a response to CO_2 concentrations in the intercellular space. For efficient CO_2 absorption, chloroplasts would expand into a sheet shape, which increases the ratio of surface area to volume (Oi *et al*., 2017), and stick to the cell periphery, especially in the areas facing the intercellular space (Sage and Sage, 2009). However, salinity or osmotic stress causes stomatal closure and decreases CO_2 concentration in the intercellular space of leaves. Then chloroplasts would become spherical by negatively responding to the low CO_2 concentration. Alternatively, the spherical shape might simply be a result of damage caused by salt stress. It is known that chloroplasts under strong or weak light conditions move by chloroplast actin (cp-actin) filaments polymerized by Chloroplast Unusual Positioning 1 (CHUP1), which anchors the chloroplast outer membrane to the plasma membrane through unknown membrane proteins (Kadota *et al*., 2009; Wada and Kong, 2018). It is also considered that chloroplasts under conditions with moderate light actively maintain their intracellular position by anchoring with actin filaments (Takagi *et al*., 2009; Wada and Kong, 2018). Although the regulatory mechanism of chloroplast shape is not well understood, salt stress might disturb the anchoring of chloroplasts to the cell periphery, and the sheeted chloroplasts would passively change to a spherical shape. Further studies are required to reveal the cytoskeleton and membrane proteins involved in chloroplast shape regulation.

Conversely, this change to a spherical shape of chloroplasts might be the acclimation to salinity stress. Chloroplasts can change their intracellular positions; they move away from light to minimize photodamage under high-intensity light irradiation (Yamada *et al*., 2009; Wada and Kong, 2018) and drought

or salinity stress (Yamada *et al*., 2009). In rice leaves, however, the mesophyll chloroplasts hardly changed their intracellular positions (Inoue and Shibata, 1974) (Fig. 4). Because the chloroplasts occupied half of the cell volume and covered most of the periphery in the rice mesophyll cell (Oi *et al*., 2017), they seemed to have less space to move inside the cell (Figs 4A and 5D). However, it is important for chloroplasts to dissipate excess light energy under salinity stress. Damage caused to chloroplasts, such as the swelling of thylakoids, under salinity is light dependent (Mitsuya *et al*., 2003*b*), and the damage is induced by excess hydrogen peroxide (H_2O_2) and H_2O_2-derived hydroxyl peroxide (Yamane *et al*., 2004). In the present study, however, thylakoids did not swell in all chloroplasts, suggesting that chloroplasts could dispose of excess light energy without changing their intracellular position. The spherical shape would reduce light absorption compared with the sheet-like shape with a higher ratio of surface area to volume (Fig. 5). The chloroplasts in rice leaves might actively change their shape to reduce light energy under salinity stress. However, the relationship between avoidance of photodamage and morphological changes (spherical shape) in chloroplasts has not been elucidated.

Overall, chloroplasts tend to become spherical under salt stress; however, they also form protrusions and pockets locally (Figs 2, 4A and 5E). The protruded bodies are in a sheet-like structure, and some chloroplasts construct pockets with a sheet structure that include cytoplasm, mitochondria or peroxisomes (Yamane *et al*., 2018). Since the protruded bodies of chloroplasts contribute to the re-assimilation of photorespired CO_2 released from mitochondria (Busch *et al*., 2013), the construction of the sheet structure and pockets could compensate for the negative effects of reducing the CO_2 absorption area by forming a spherical shape under salinity stress. Further studies are required to elucidate the relationship between the sub-structural changes in chloroplasts and photosynthesis.

In conclusion, chloroplasts became spherical under salinity stress without increasing in volume. Previous views of swelling in chloroplasts were misinterpretations based on 2-D observations, suggesting that the use of 3-D analysis would be useful for future studies to prevent similar misinterpretations. The physiological significance of this morphological change remains unclear and, therefore, the relationship between chloroplast ultrastructure and their functionality under salinity stress should be further investigated in the future.

SUPPLEMENTARY DATA

Supplementary data are available online at https://academic.oup.com/aob and consist of the following. Videos S1–S6: all actual transverse slices, virtual orthogonal slice and 3-D reconstructed models of chloroplasts in a whole rice mesophyll cell; S1, C1; S2, C2; S3, C3; S4, N1; S5, N2; and S6, N3 in Figs 3 and 4.

FUNDING

This work was supported by the Nagoya University microstructural characterization platform as a programme of the 'Nanotechnology Platform' of the Ministry of Education, Culture, Sports, Science and Technology (MEXT), Japan. In addition, this work was partially supported by the Japan Society for the Promotion of Science (JSPS) KAKENHI. Grant nos JP19K15823 (to T.O.), JP18K05603 (to K.Y.) and JP17H03757 (to M.T.).

ACKNOWLEDGEMENTS

We thank Mr Tsubasa Tanizawa for processing the image data, and Dr Hiroshi Miyake for reviewing the manuscript.

LITERATURE CITED

Bourett TM, Czymmek KJ, Howard RJ. 1999. Ultrastructure of chloroplast protuberances in rice leaves preserved by high-pressure freezing. *Planta* **208**: 472–479.

Busch FA, Sage TL,. Cousins AB, Sage RF. 2013. C_3 plants enhance rates of photosynthesis by reassimilating photorespired and respired CO_2. *Plant, Cell & Environment* **36**: 200–212.

Chaves MM, Flexas J, Pinheiro C. 2009. Photosynthesis under drought and salt stress: regulation mechanisms from whole plant to cell. *Annals of Botany* **103**: 551–560.

Chiba A, Ishida H, Nishizawa NK, Makino A, Mae T. 2003. Exclusion of ribulose-1,5-bisphosphate carboxylase/oxygenase from chloroplasts by specific bodies in naturally senescing leaves of wheat. *Plant & Cell Physiology* **44**: 914–921.

Chonan N. 1967. Studies on the photosynthetic tissues in the leaves of cereal crops: III. The mesophyll structure of rice leaves inserted at different levels of the shoot. *Japanese Journal of Crop Science* **36**: 291–296.

Gray JC, Hansen MR, Shaw DJ, Graham K, Dale R, Smallman P, Natesan SK A, Newell CA. 2012. Plastid stromules are induced by stress treatments acting through abscisic acid. *Plant Journal* **69**: 387–398.

Hillel D. 2000. *Salinity management for sustainable irrigation: integrating science, environment, and economics (environmentally and socially sustainable development series)*. Washington, DC:The World Bank.

Hughes L, Hawes C, Monteith S, Vaughan S. 2014. Serial block face scanning electron microscopy – the future of cell ultrastructure imaging. *Protoplasma* **251**: 395–401.

Inoue Y, Shibata K. 1974. Comparative examination of terrestrial plant leaves in terms of light-induced absorption changes due to chloroplast rearrangements. *Plant & Cell Physiology* **15**: 717–721.

Ishida H, Izumi M, Wada S, Makino A. 2014. Roles of autophagy in chloroplast recycling. *Biochimica et Biophysica Acta* **1837**: 512–521.

Kadota A, Yamada N, Suetsugu N, *et al.* 2009. Short actin-based mechanism for light-directed chloroplast movement in *Arabidopsis*. *Proceedings of the National Academy of Sciences, USA* **106**: 13106–13111.

Knott G, Marchman H, Wall D, Lich B. 2008. Serial section scanning electron microscopy of adult brain tissue using focused ion beam milling. *Journal of Neuroscience* **28**: 2959–2964.

Köhler RH, Hanson MR. 2000. Plastid tubules of higher plants are tissue-specific and developmentally regulated. *Journal of Cell Science* **113**: 81–89.

Lucas MS, Günthert M, Gasser P, Lucas F, Wepf R. 2012. Bridging microscopes: 3D correlative light and scanning electron microscopy of complex biological structures. *Methods in Cell Biology* **111**: 325–356.

Mae T, Ohira K. 1981. The remobilization of nitrogen related to leaf and senescence in rice plants (*Oryza* sativa L.). *Plant & Cell Physiology* **22**: 1067–1074.

Mitsuya S, Kawasaki M, Taniguchi M, Miyake H. 2003*a*. Relationship between salinity-induced damages and aging in rice leaf tissues. *Plant Production Science* **6**: 213–218.

Mitsuya S, Kawasaki M, Taniguchi M, Miyake H. 2003*b*. Light dependency of salinity-induced chloroplast degradation. *Plant Production Science* **6**: 219–223.

Oi T, Enomoto S, Nakao T, Arai S, Yamane K, Taniguchi M. 2017. Three-dimensional intracellular structure of a whole rice mesophyll cell observed with FIB-SEM. *Annals of Botany* **120**: 21–28.

Parida AK, Das AB. 2005. Salt tolerance and salinity effects on plants: a review. *Ecotoxicology and Environmental Safety* **60**: 324–349.

Rahman S, Matsumuro T, Miyake H, Takeoka Y. 2000. Salinity-induced ultrastructural alterations in leaf cells of rice (*Oryza sativa* L.). *Plant Production Science* **3**: 422–429.

Sage TL, Sage RF. 2009. The functional anatomy of rice leaves: implications for refixation of photorespiratory CO_2 and efforts to engineer C_4 photosynthesis into rice. *Plant & Cell Physiology* **50**: 756–772.

Schindelin J, Arganda-Carreras I, Frise E, *et al.* 2012. Fiji: an open-source platform for biological-image analysis. *Nature Methods* **9**: 676–682.

Takagi S, Takamatsu H, Sakurai-Ozato N. 2009. Chloroplast anchoring: its implications for the regulation of intracellular chloroplast distribution. *Journal of Experimental Botany* **60**: 3301–3310.

Wada M, Kong SG. 2018. Actin-mediated movement of chloroplasts. *Journal of Cell Science* **131**: jcs210310.

Yamada M, Kawasaki M, Sugiyama T, Miyake H, Taniguchi M. 2009. Differential positioning of C_4 mesophyll and bundle sheath chloroplasts: aggregative movement of C_4 mesophyll chloroplasts in response to environmental stresses. *Plant & Cell Physiology* **50**: 1736–1749.

Yamane K, Kawasaki M, Taniguchi M, Miyake H. 2003. Differential effect of NaCl and polyethylene glycol on the ultrastructure of chloroplasts in rice seedlings. *Journal of Plant Physiology* **160**: 573–575.

Yamane K, Rahman MS, Kawasaki M, Taniguchi M, Miyake H. 2004. Pretreatment with antioxidants decreases the effects of salt stress on chloroplast ultrastructure in rice leaf segments (*Oryza* sativa L.). *Plant Production Science* **7**: 292–300.

Yamane K, Kawasaki M, Taniguchi M, Miyake H. 2008. Correlation between chloroplast ultrastructure and chlorophyll fluorescence characteristics in the leaves of rice (*Oryza sativa* L.) grown under salinity. *Plant Production Science* **11**: 139–145.

Yamane K, Mitsuya S, Taniguchi M, Miyake H. 2012. Salt-induced chloroplast protrusion is the process of exclusion of ribulose-1,5-bisphosphate carboxylase/oxygenase from chloroplasts into cytoplasm in leaves of rice. *Plant, Cell & Environment* **35**: 1663–1671.

Yamane K, Oi T, Enomoto S, Nakao T, Arai S, Miyake H, Taniguchi M. 2018. Three-dimensional ultrastructure of chloroplast pockets formed under salinity stress. *Plant, Cell & Environment* **41**: 563–575.